<div align="center">**Supporting Information**</div>

High Spatial Resolution X-ray Scintillators Based on a 2D Copper(I) Iodide Hybrid.

Han-Jiang Yang,[†, ‡] Weijia Xiang,[§] Xiangzhou Zhang,[§] Jin-Yun Wang,[†] Liang-Jin Xu[†,‡,⊥,*] Zhong-Ning Chen[†,‡,⊥,*]

[†] *State Key Laboratory of Structural Chemistry, Fujian Institute of Research on the Structure of Matter, Chinese Academy of Sciences, Fuzhou 350002, China*
[‡] *College of Chemistry and Materials Science, Fujian Normal University, Fuzhou 350007, China*
[⊥] *Fujian Science & Technology Innovation Laboratory for Optoelectronic Information of China, Fuzhou 350108, China*

[§] *Institute for Advanced Interdisciplinary Research (iAIR), University of Jinan, Jinan 250022, China*

1. Reagents:

cis-2,6-Dimethylmorpholine ($C_6H_{13}NO$, 99%) was purchased from Bide Reagent Co., Ltd. Cuprous(I) iodide (CuI, 98%), hypophosphorous acid (H_3PO_2, 50% wt in water) and hydroiodic acid (HI, 47wt% in water) were purchased from Macklin Reagent Co., Ltd. Acetonitrile (C_2H_3N, 99.5%) was purchased from Sino Reagent Co., Ltd. All reagents and solvents were used without further purification.

2. Synthesis:

Synthesis of $(CISDM)_4[Cu_4I_8]\cdot2H_2O$. First, $C_6H_{13}NO$ (2.6 mmol, 300 mg) and CuI (0.86 mmol, 165 mg) were dissolved in mixed solvents of CH_3CN (6 mL), H_3PO_2(1 mL) and HI (1mL) at 75°C to form a clear saturation precursor solution. The solution was allowed to cool slowly to room temperature. Colorless transparent sheet-like crystals of $(CISDM)_4[Cu_4I_8]\cdot2H_2O$ were grown upon standing for 48 h.

3. Characterizations

Single-crystal X-ray diffraction (SCXRD). Single-crystal X-ray diffraction (SCXRD) data were recorded using Bruker D8 ADVANCE with a graphite monochromated Mo-Kα (λ = 0.71073 Å) radiation. The structure was solved by the direct method using a SHELXL-97 program.

Powder X-ray Diffraction (PXRD). PXRD patterns were recorded using Rigaku MiniFlex 600 with a Cu-Kα (λ = 1.54184 Å) radiation in the range of 10–50° at a scan rate of 5° min^{-1}.

Photoluminescence (PL) Steady State Studies. PL properties, including emission and excitation spectra in solid state at room temperature, were measured on an FLS 1000 Edinburgh fluorescence spectrometer. In addition, PL quantum efficiency measurements were performed using the same light source with an additional integrating sphere by FLS 1000 Edinburgh fluorescence spectrometer. The PLQY was calculated by following equation (S1):

$$\eta = \left(\int L_{direct} - \int L_{blank} \right) / \left(\int E_{without} - \int E_{direct} \right) \qquad \text{(S1)}$$

where η is the photoluminescent quantum yield, L_{direct} is the complete emission spectrum of the sample collected by using the integrating sphere, L_{blank} is the emission spectrum of the blank sample, E_{direct} is the emission spectra of the excitation light, recorded with the sample in place, and $E_{without}$ is the emission spectrum of excitation light, recorded with the equipment blank in place. The part $\left(\int L_{direct} - \int L_{blank} \right)$ expresses the photons emitted by our sample, and $\left(\int E_{without} - \int E_{direct} \right)$ means the photons emitted by excitation light source. Time-resolved emission data were collected at room temperature using the FLS 1000 spectrofluorometer with a microsecond light source. The dynamics of emission decay were monitored by using the FLS 1000 time-correlated single-photon counting capability (2000 channels; 200 μs window) with data collection for 100,00 counts.

Ultraviolet-visible (UV-Vis) absorption. Ultraviolet-visible (UV-Vis) absorption spectra were obtained using a PerkinElmer LAMBDA 950 UV-Vis spectrophotometer using $BaSO_4$ powder as a reflectance reference. The absorption spectra were obtained using powders from single crystals.

Thermogravimetric analysis (TGA). The thermogravimetric analyses (TGA) were measured on a Netzsch STA449F3 instrument heated from 25 to 800°C at a ramp rate of 5.00°C min^{-1} under a nitrogen flux of 100 mL min^{-1}.

Measurement of Radioluminescence Spectra Intensity. FLS 920 spectrofluorometer (Edinburgh Instruments Ltd., U. K.) equipped with an X-ray tube (TUB00154-9I-W06, Mo target and tube voltage of 70 kV) was used to measure the RL spectra. The corresponding RL intensity can be calculated by integrating the RL spectra.

Calculation of Light Yield. The commercial CsI:Tl scintillator was used as a reference to calibrate the light yield of (CISDM)$_4$[Cu$_4$I$_8$]·2H$_2$O scintillator. (CISDM)$_4$[Cu$_4$I$_8$]·2H$_2$O and the CsI:Tl scintillators were set at the same position to measure the RL spectra. Then the corresponding photon counting results were obtained by integrating the RL spectra. Light yield was defined as the ratio of photon numbers emitted from the luminescent sites to the total absorbed X-ray energy, and it represents an internal X-ray conversion efficiency. Therefore, the emission photon counts of scintillators should be normalized to the same X-ray attenuation. In addition, the response of CsI:Tl was >1.31 times higher than that of (CISDM)$_4$[Cu$_4$I$_8$]·2H$_2$O. Based on this, the calculated light yield of (CISDM)$_4$[Cu$_4$I$_8$]·2H$_2$O scintillator was 41,042 photons MeV^{-1}. In detail, the LY of (CISDM)$_4$[Cu$_4$I$_8$]·2H$_2$O can be obtained from the equation (S2):

$$\frac{LY_{(CISDM)_4Cu_4I_8\cdot2H_2O}}{LY_{CsI:Tl}} = \frac{R_{(CISDM)_4Cu_4I_8\cdot2H_2O}}{R_{CsI:Tl}} \times \frac{\int I_{CsI:Tl}(\lambda)S(\lambda)d\lambda / \int I_{CsI:Tl}(\lambda)d\lambda}{\int I_{(CISDM)_4Cu_4I_8\cdot2H_2O}(\lambda)S(\lambda)d\lambda / \int I_{(CISDM)_4Cu_4I_8\cdot2H_2O}(\lambda)d\lambda} \times \frac{S_{CsI:Tl}}{S_{(CISDM)_4Cu_4I_8\cdot2H_2O}}$$

(S2)

Microscope image of (CISDM)$_4$[Cu$_4$I$_8$]·2H$_2$O. X-ray imaging was performed on an inverted fluorescent microscope (Axio Vert. A1,Carl Zeiss) coupling with a portable X-ray tube (MAGPRO, Moxtek). Thevoltage divided by current of the X-ray tube was set to 50 kV 100 μA^{-1} under objective lens of magnifications at 5×.

Calculation of Modulation Transfer Function. Modulation transfer function (MTF) was defined as the transfer capability of the input signal modulation of spatial frequency, which generally acts as the evaluation index of the spatial resolution

performance of imaging system. MTF = output contrast of the image/enter the contrast of the image. Since the contrast of the output image was always smaller than that of the input image, the MTF value was thus between 0 and 1. When the MTF value decreases to 0.2, the spatial resolution can be determined by the corresponding spatial frequency. Here, slanted-edge method was adopted to calculate the MTF curve. An X-ray image using thin slice of Aluminum (Al) with sharp edge was taken, the edge spread function (ESF) can be obtained from the slanted-edge profile of this X-ray image. The MTF can be calculated by the following equation (S3):

$$MTF(v) = F[LSF(x)] = F\left(\frac{dESF(x)}{dx}\right)$$ (S3)

where v is the spatial frequency and x is the position of pixels, and the line spread function (LSF) was the derivative of ESF and the MTF was the Fourier transform of LSF. Then MTF calculation on image was operated through software Image J (https://imagej.en.softonic.com/).

4. Calculation methods.

The energy band structures and density of states (DOS) were theoretically calculated by using the first-principles plane-wave pseudopotential method with the code CASTEP provided by the software Materials Studio v7.0.[1,2] The generalized gradient approximation (GGA) functional of Perdew–Burke–Ernzerh (PBE)[3] was employed for the geometry optimization and energy calculation. The precise of the plane wave basis sets was set as 400 eV cutoff energy. The k-point mesh in the Brillouin zone was represented as 2*2*2 of the Monkhorst-Pack grid and the ultra soft pseudopotentials in the reciprocal space was used. The other calculating parameters and convergent criteria were set the default values of the CASTEP code.

5. Supplementary Tables

Table S1. The Crystallographic Data of $(CISDM)_4[Cu_4I_8]\cdot2H_2O$

Compound	$(CISDM)_4[Cu_4I_8]\cdot2H_2O$
Empirical formula	$C_3H_{6.50}Cu_{0.50}IN_{0.50}O_{0.75}$
Temperature / K	301

Crystal system	Monoclinic
Space group	Cm
a / Å	7.3770 (7)
b / Å	22.997 (2)
c / Å	7.4158 (7)
$\alpha/°$	90
$\beta/°$	105.315 (3)
$\gamma/°$	90
Volume / Å^3	1213.4 (2)
Z	8
ρ_{calc} / mg m^{-3}	2.411
μ / mm^{-1}	6.85
Rdiation(λ) / Å	0.71073
R_1 [a]	0.029
wR_2 [b]	0.111
GOF	0.95

a) $R1 = \Sigma|F_o-F_c|/\Sigma F_o$,   b) $wR2 = \Sigma[w(F_o{}^2-F_c{}^2)^2]/\Sigma[w(F_o)^2)]^{1/2}$

Table S2. The bond lengths (Å) and angles (°) of $(CISDM)_4[Cu_4I_8]\cdot 2H_2O$

Bond	Distance(Å)
I3—Cu2	2.705 (2)
I3—Cu1^i	2.7272 (19)
I2—Cu2	2.6344 (12)
I2—Cu1	2.6538 (11)
I1—Cu1	2.730 (2)
I1—Cu2^{ii}	2.801 (3)
Cu2—I2^{iii}	2.6344 (12)
Cu2—Cu1	2.740 (2)
Cu2—I1^{iv}	2.801 (3)
Cu1—I2^{iii}	2.6538 (11)
Cu1—I3^v	2.7272 (19)
C4—O1	1.429 (11)
C4—C5	1.482 (17)
C4—C3	1.519 (13)

C4—H4A	0.9800
O1—C1	1.458 (12)
C3—N1	1.470 (14)
C3—H3A	0.9700
C3—H3B	0.9700
C1—C2	1.490 (13)
C1—C6	1.518 (15)
C1—H1A	0.9800
C5—H5A	0.9600
C5—H5B	0.9600
C5—H5C	0.9600
N1—C2	1.492 (15)
N1—H1B	0.8600
C6—H6A	0.9600
C6—H6B	0.9600
C6—H6C	0.9600
C2—H2A	0.9700
C2—H2B	0.9700

Atoms	Angle(°)
Cu2—I3—Cu1^{i}	173.76 (7)
Cu2—I2—Cu1	62.41 (4)
Cu1—I1—Cu2^{ii}	176.94 (9)
I2—Cu2—I2^{iii}	118.22 (8)
I2—Cu2—I3	107.28 (6)
I2^{iii}—Cu2—I3	107.28 (6)
I2—Cu2—Cu1	59.14 (4)
I2^{iii}—Cu2—Cu1	59.14 (4)
I3—Cu2—Cu1	122.91 (9)
I2—Cu2—I1^{iv}	106.25 (6)
I2^{iii}—Cu2—I1^{iv}	106.25 (6)
I3—Cu2—I1^{iv}	111.63 (8)
Cu1—Cu2—I1^{iv}	125.46 (8)

I2—Cu1—I2^{iii}	116.84 (7)
I2—Cu1—I3^{v}	108.27 (5)
I2^{iii}—Cu1—I3^{v}	108.27 (5)
I2—Cu1—I1	107.37 (6)
I2^{iii}—Cu1—I1	107.37 (6)
I3^{v}—Cu1—I1	108.45 (7)
I2—Cu1—Cu2	58.45 (4)
I2^{iii}—Cu1—Cu2	58.45 (4)
I3^{v}—Cu1—Cu2	129.15 (8)
I1—Cu1—Cu2	122.40 (8)
O1—C4—C5	107.6 (8)
O1—C4—C3	109.3 (7)
C5—C4—C3	110.9 (10)
O1—C4—H4A	109.6
C5—C4—H4A	109.6
C3—C4—H4A	109.6
C4—O1—C1	110.8 (7)
N1—C3—C4	110.7 (8)
N1—C3—H3A	109.5
C4—C3—H3A	109.5
N1—C3—H3B	109.5
C4—C3—H3B	109.5
H3A—C3—H3B	108.1
O1—C1—C2	108.7 (8)
O1—C1—C6	106.2 (8)
C2—C1—C6	109.3 (9)
O1—C1—H1A	110.8
C2—C1—H1A	110.8
C6—C1—H1A	110.8
C4—C5—H5A	109.5
C4—C5—H5B	109.5
H5A—C5—H5B	109.5
C4—C5—H5C	109.5
H5A—C5—H5C	109.5

H5B—C5—H5C	109.5
C3—N1—C2	111.5 (7)
C3—N1—H1B	124.3
C2—N1—H1B	124.3
C1—C6—H6A	109.5
C1—C6—H6B	109.5
H6A—C6—H6B	109.5
C1—C6—H6C	109.5
H6A—C6—H6C	109.5
H6B—C6—H6C	109.5
C1—C2—N1	110.9 (9)
C1—C2—H2A	109.5
N1—C2—H2A	109.5
C1—C2—H2B	109.5
N1—C2—H2B	109.5
H2A—C2—H2B	108.1

**Table S3.** Radioluminescence properties of recently reported metal halide scintillators.

scintillators	decay times (μs)	ligh yields (photons MeV^{-1})	detection limit (nGy$_{air}$ s^{-1})	spatial resolution (lp mm^{-1})	imaging	Ref
$Cs_3Cu_2I_5$ NC	1.92	79279	/	0.32 mm	NC films	[4]
$Cs_3Cu_2I_5$ SC	0.912	30000	158		SC	[5]
$Cs_3Cu_2I_5$:Tl$^+$ NC	7.66	48800	305	16.3		[6]
$Cs_3Cu_2I_5$:In$^+$ SC	0.557, 3.746	53000	96	18	SC	[5]
Rb_2CuCl_3	11.3	16600	88.5	/	/	[7]
Rb_2CuBr_3	41.4	91056	121.5	/	/	[8]
K_2CuBr_3	64.3	23806	132.8	/	/	[9]
Cs_2AgI_3:Cu$^+$	0.193	82900	77.8	16.2	PDMS composite film	[10]
$Cs_2Ag_{0.6}Na_{0.4}In_{0.85}Bi_{0.15}Cl_6$	/	39000±7000	19	4.4	Wafer	[11]
Rb_2AgBr_3	0.00531	25600	19	10.2	Film	[12]
$(C_{38}H_{34}P_2)MnBr_4$	318	79800 (SC) 66256 (film)	461.1	0.322 mm	PDMS composite film	[13]
TPP_2MnBr_4	265	7800±2000	8.8	15.7	CW	[14]
$(ETP)_2MnBr_4$	295	3500±2000	103	13.41	Transparent glass	[15]
$(C_{24}H_{20}P)_2MnBr_4$	316.45	/	608	14.5	TPU composite film	[16]

$C_4H_{12}NMnCl_3$	758.95	50500	36.9	/	SO composite film	[17]
$(C_8H_{20}N)_2MnBr_4$	442.52	24400	24.2	5	SO composite film	[17]
TEA_2MnI_4	/	26288	8.8	25	SC	[18]
$(C_8H_{17}NH_3)_2SnBr_4$	3.34	/	10423	/	PMMA composite film	[19]
$(PPN)_2SbCl_5$	/	49000	191.4	/	SC	[20]
Cs_2ZrCl_6		49400	65	18	PDMS composite film	[21]
$(Bmpip)_2Cu_2Br_4$	/	16000	710	/	/	[22]
$(DIET)_3Cu_3Br_3$	0.6	20000$\pm$700	189	11.71	PDMS composite film	[23]
$(AEP)_2Cu_2I_6 \cdot 2I \cdot 2H_2O$	3.18	55650	/	2.8	PMMA composite film	[24]
$(TBA)CuCl_2$	28.7	23373	/	/	PVDF composite film	[25]
$(TBA)CuBr_2$	232.05	24134	/	/	PVDF composite film	[25]
$(C_8H_{20}N)_2Cu_2Br_4$	56	91750(SC) 69750 (CW)	52.1	9.54	CW	[26]
$(CISDM)_4Cu_4I_8 \cdot 2H_2O$	/	41042	86.8	108	SC	This work

Note: "NC", nanocrystal; "SC", single crystal; "CANIBC", "PMMA", polymethyl methacrylate; "PDMS", polydimethylsiloxane; "TPU", thermoplastic polyurethane; "SO",sucrose octaacetate; "PVDF", polyvinylidene fluoride; "CW", Ceramic wafer.
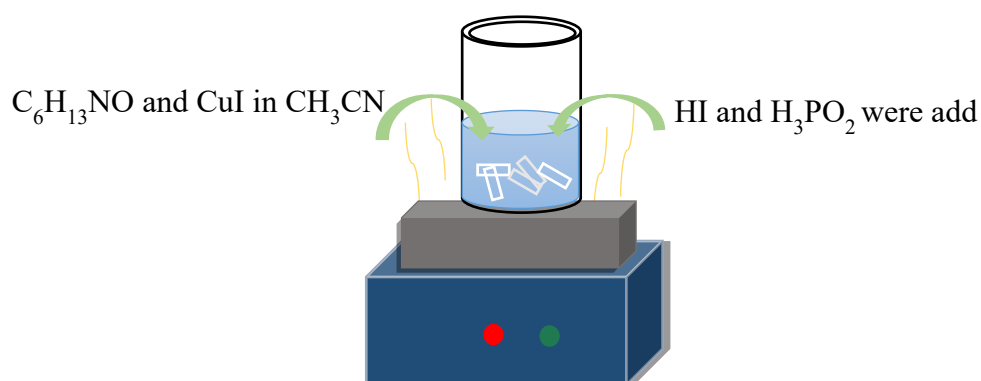
Figure S1. Illustration of solution crystal growth of $(CISDM)_4[Cu_4I_8]\cdot2H_2O$.
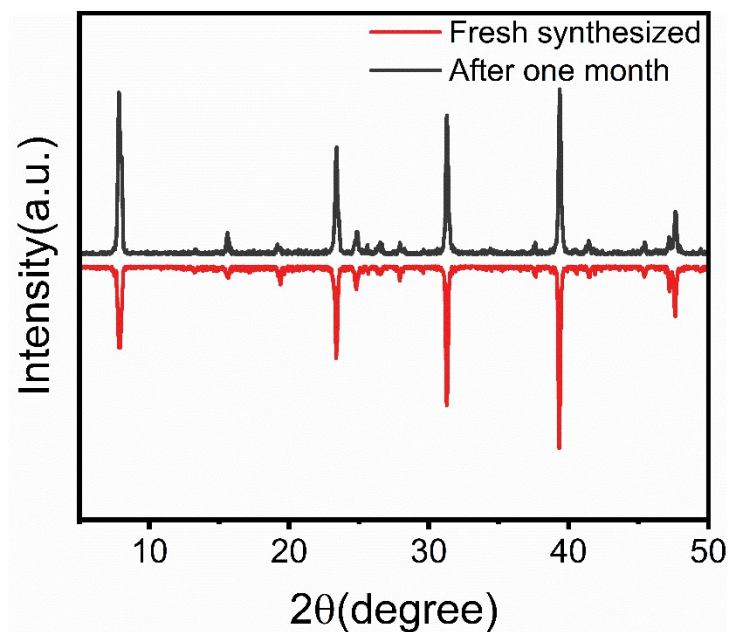
Figure S2. PXRD patterns of (CISDM)$_4$[Cu$_4$I$_8$]·2H$_2$O upon exposed to air for one month.
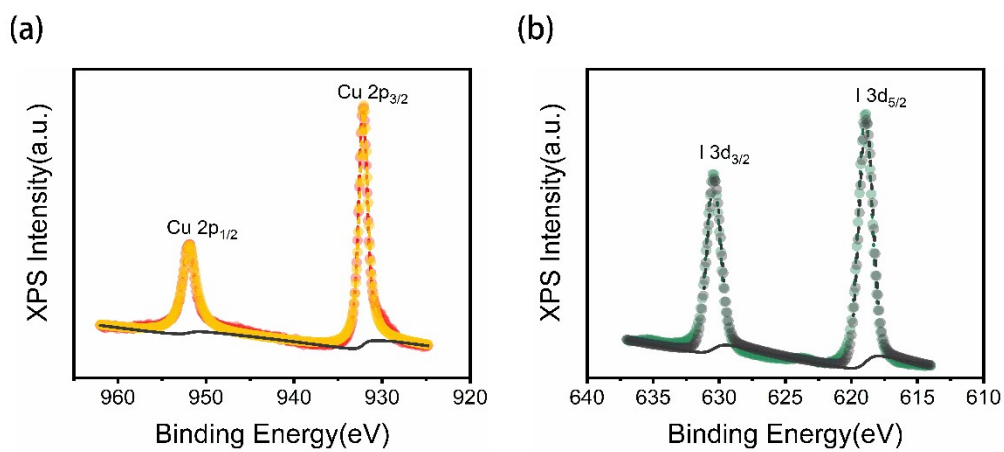
Figure S3. XPS spectra for (CISDM)$_4$[Cu$_4$I$_8$]·2H$_2$O single crystals. (a) Cu 2p. (b) I 3d.
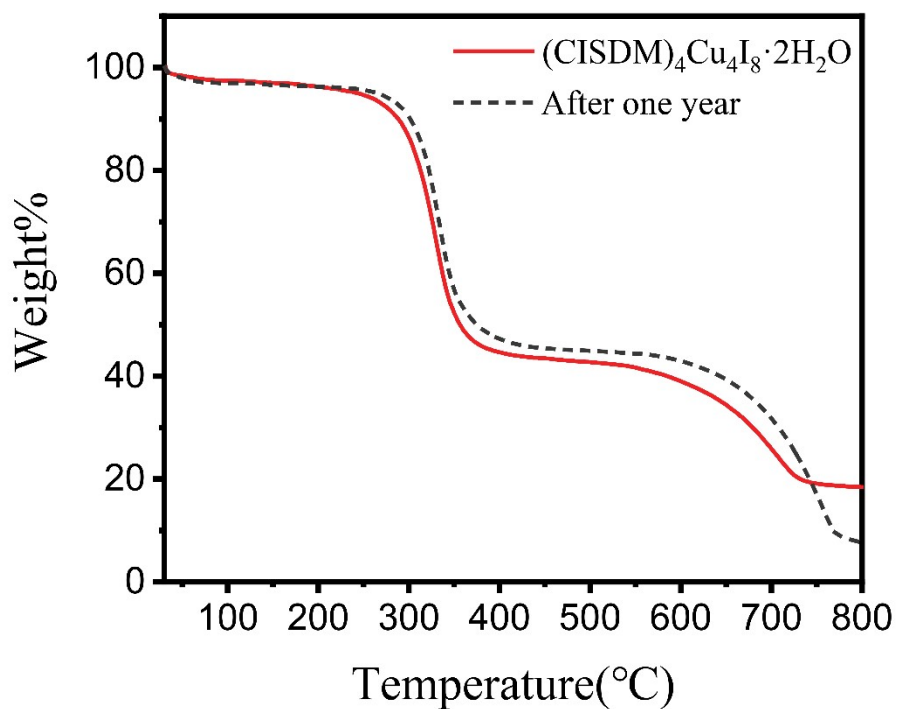
Figure S4. The TGA curve of $(CISDM)_4[Cu_4I_8]·2H_2O$ and upon exposed to air for one year.
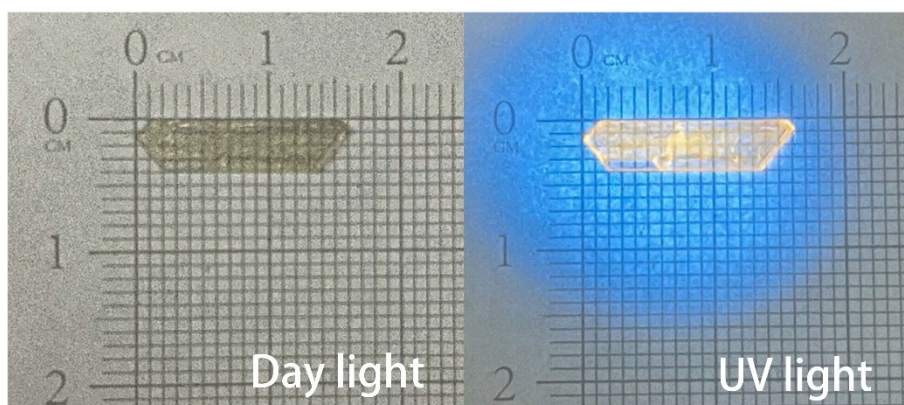
Figure S5. Optical images of $(CISDM)_4[Cu_4I_8]·2H_2O$ single crystal under daylight (left) and UV light (right) with the size of $1.6 × 0.4 × 0.01$ cm^3.
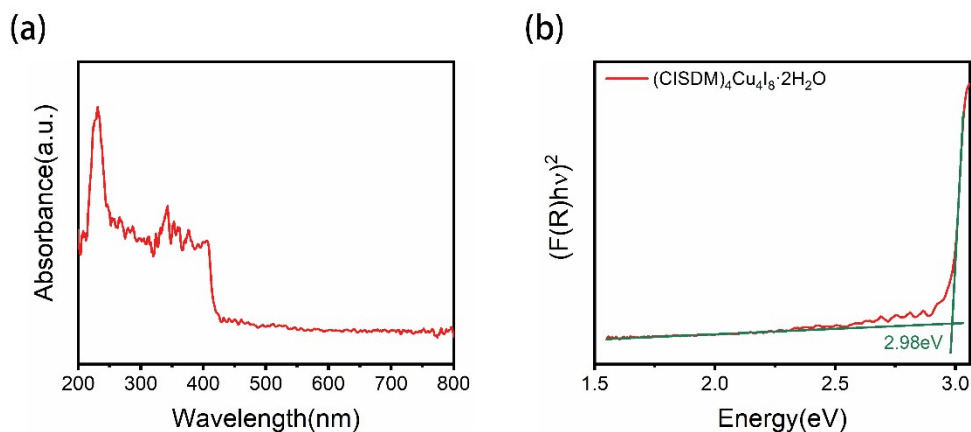
Figure S6. (a) Room-temperature absorption spectrum of $(CISDM)_4[Cu_4I_8]\cdot 2H_2O$ powder. (b) The $(Ah\upsilon)^2 \sim h\upsilon$ curve of $(CISDM)_4[Cu_4I_8]\cdot 2H_2O$ with a band gap of 2.98 eV.
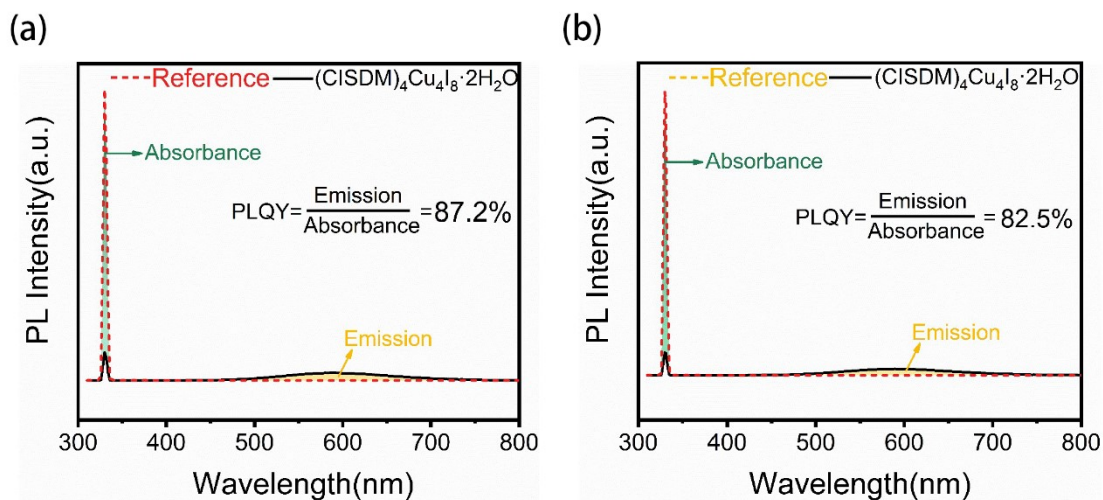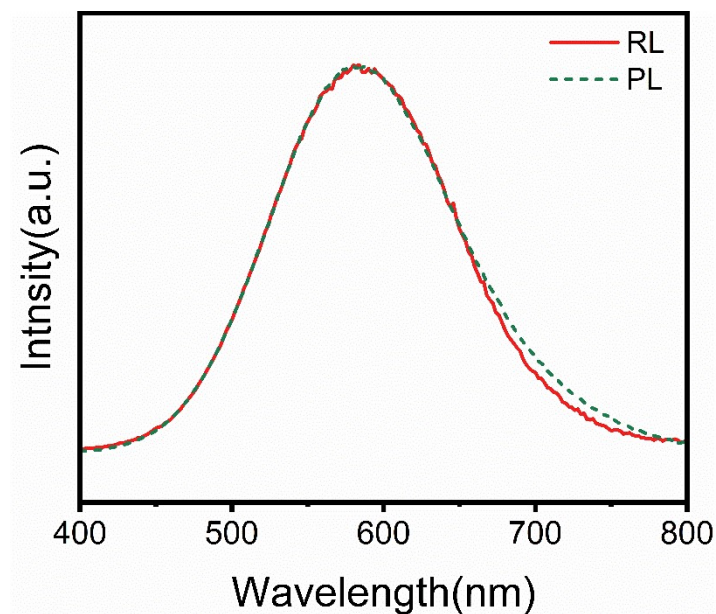

Figure S7. The PLQY spectra of $(CISDM)_4[Cu_4I_8]\cdot 2H_2O$ fresh crystals and upon exposed to air for one months.
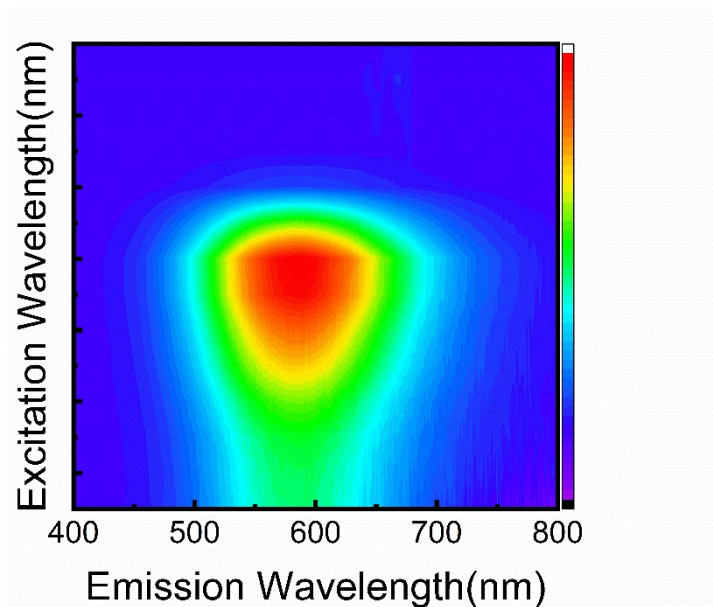
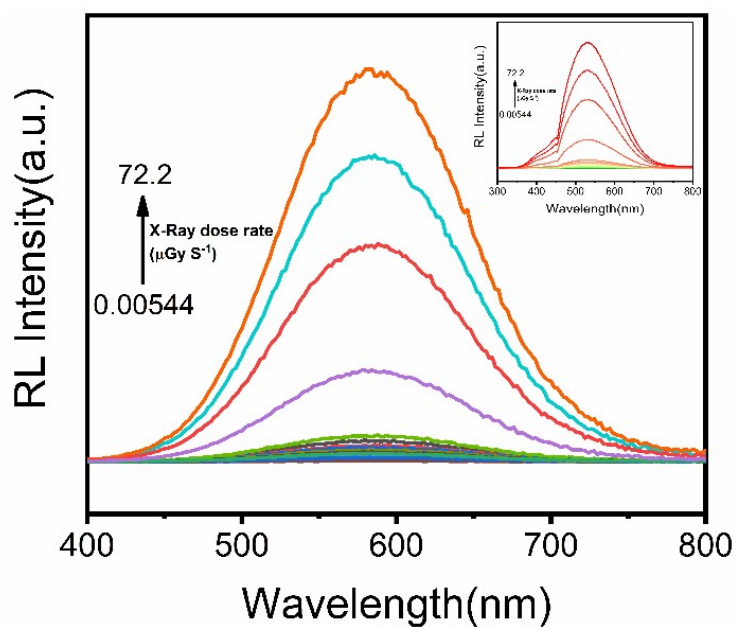**Figure S8.** PL and PLE contour mappings of (CISDM)$_4$[Cu$_4$I$_8$]·2H$_2$O single crystals.
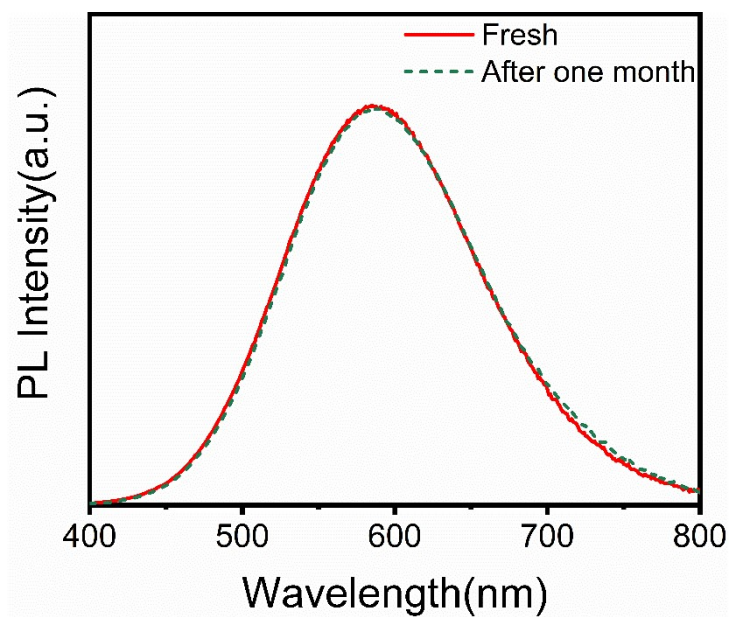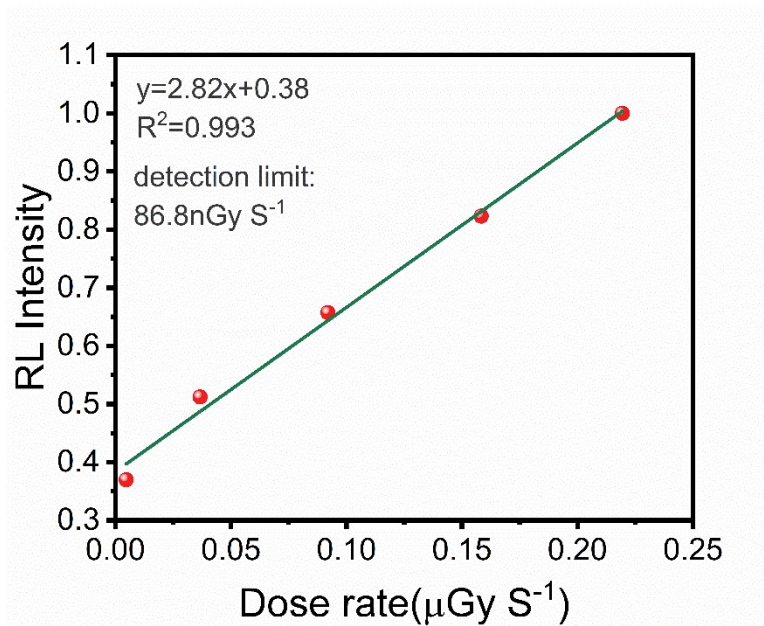

**Figure S9.** PL spectra of (CISDM)$_4$[Cu$_4$I$_8$]·2H$_2$O fresh crystals and upon exposed to air for one months.

**Figure S10.** The radioluminescence and photoluminescence spectra of $(CISDM)_4[Cu_4I_8] \cdot 2H_2O$.

Figure S11. X-ray dose rate dependent radioluminescence of $(CISDM)_4[Cu_4I_8] \cdot 2H_2O$ and CsI:Tl.

Figure S12. The detection limit measurement under low X-ray dose for a flexible scintillator containing $(CISDM)_4[Cu_4I_8]\cdot 2H_2O$.
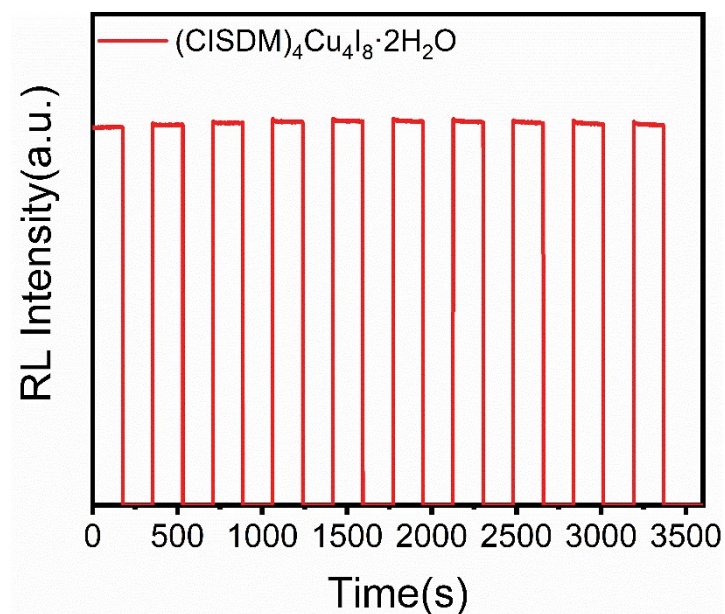
Figure S13. Photostability of $(CISDM)_4[Cu_4I_8]\cdot 2H_2O$ scintillator at an X-ray dose of 133.64 μGy s^{-1} for 1 h.
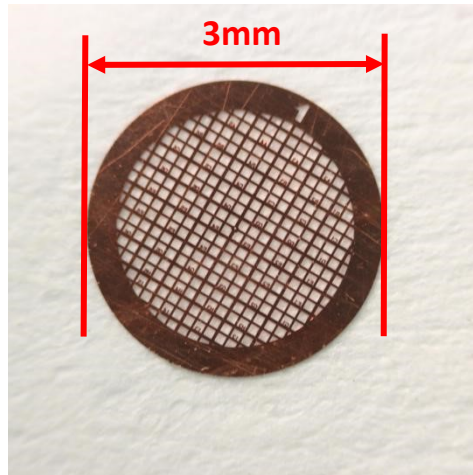
Figure S14. Photograph of a copper grid for X-ray imaging.

Reference

[1]. S. J. Clark, M. D. Segall, C. J. Pickard, P. J. Hasnip, M. J. Probert, K. Refson, M. C. Payne, Z. Kristallogr. 2005, **220**, 567-570.

[2]. K. Refson, S. J. Clark, P. R. Tulip, *Phys. Rev.* B 2006, **73**, 155114-155112.

[3]. J. P. Perdew, K. Burke, M. Ernzerhof, *Phys. Rev. Lett*. 1996, **77**, 3865-3868.

[4]. L.Y. Lian, M.Y. Zheng, W.Z. Zhang, L.X. Yin, X.Y. Du, P. Zhang, X.W. Zhang, J.B.Gao, D.L.Zhang, L. Gao, G.D. Niu, H.S. Song, R. Chen, X.Z. Lan, J. Tang, J.B. Zhang, *Adv.Sci*. 2020, **7**, 2000195.

[5]. Q. Wang, Q. Zhou, M. Nikl, J.W. Xiao, R. Kucerkova, A. Beitlerova, V. Babin, P. Prusa,V. Linhart, J.K. Wang, X.M. Wen, G.D. Niu, J. Tang, G.H. Ren, Y.T. Wu, *Advanced Optical Materials*.2022, **10**, 2200304.

[6]. X. Hu, P. Yan, P. Ran, L. Lu, J. Leng, Y.M. Yang, X. Li, *J. Phys. Chem. Lett*. 2022, **13**,2862-2870.

[7]. X. Zhao, G.D. Niu, J.S. Zhu, B. Yang, J.H. Yuan, S.R. Li, W.R. Gao, Q.S. Hu, L.X. Yin,K.H. Xue, E. Lifshitz, X.S. Miao, J. Tang, *J. Phys. Chem. Lett*. 2020, **11**, 1873-1880.

[8]. B. Yang, L. Yin, G. Niu, J.H. Yuan, K.H. Xue, Z. Tan, X.S. Miao, M. Niu, X. Du, H.Song, E. Lifshitz, J. Tang, *Advanced Materials*. 2019, **31**, e1904711.

[9]. W.R. Gao, G.D. Niu, L.X. Yin, B. Yang, J.H. Yuan, D.D. Zhang, K.H. Xue, X.S. Miao,Q.S. Hu, X.Y. Du, J. Tang, *ACS Appl. Electron. Mater*. 2020, **2**, 2242-2249.

[10]. T.Y. He, Y. Zhou, X.J. Wang, J. Yin, A. Gutiérrez, L., J.X. Wang, Y.H. Zhang, O.M.Bakr, O.F. Mohammed, *ACS Energy Lett*. 2022, **7**, 2753-2760.

[11]. W.J. Zhu, W.B. Ma, Y.R. Su, Z. Chen, X.Y. Chen, Y.G. Ma, L.Z. Bai, W.G. Xiao, T.Y.Liu, H.M. Zhu, X.F. Liu, H.F. Liu, X. Liu, Y.M. Yang, *Light Sci. Appl.* 2020, **9**, 112.

[12]. M.Y. Zhang, X.M. WANG, B. Yang, J.S. Zhu, G.D. Niu, H.D. Wu, L.X. Yin, X.Y. Du,M. Niu, Y.S. Ge, Q.G. Xie, Y.F. Yan, J. Tang, *Adv. Funct. Mater*. 2020, **31**, 2007921.

[13]. L.J. Xu, X.S. Lin, Q.Q. He, M. Worku, B.W. Ma, *Nature Communications*. 2020, **11**, 4329.

[14]. K. Han, K. Sakhatskyi, J.C. Jin, Q. Zhang, M.V. Kovalenko, Z.G. Xia, *Advanced Materials*. 2022,**34**, e2110420.

[15]. B.H. Li, Y. Xu, X.L. Zhang, K. Han, J.C. Jin, Z.G. Xia, *Advanced Optical Materials*. 2022, **10**,2102793.

[16]. K.Y. Xia, P. Ran, W.W. Wang, J.W. Yu, G.P. Xu, K. Wang, X.D. Pi, Q.Q. He, Y. Yang,J. Pan, *Advanced Optical Materials*. 2022, 10, 2201028.

[17]. T.M. Jiang, W.B. Ma, H. Zhang, Y. Tian, G. Lin, W.G. Xiao, X. Yu, J.B. Qiu, X.H. Xu,Y. Yang, D.X. Ju, *Adv. Funct. Mater*. 2021, **31**, 2009973.

[18]. Zhang, Z. Z.Wei, J. H.Luo, J. B.Wang, X. D.He, Z. L.Kuang, D. B.*ACS Appl.Mater.Interfaces*,2022,**14**,47913-47921.

[19]. J.T. Cao, Z. Guo, S. Zhu, Y. Fu, H. Zhang, Q. Wang, Z.J. Gu, *ACS Appl. Mater.Interfaces* 2020, **12**, 19797-19804.

[20]. He, Q. Q.Zhou, C. K.Xu, L. J.Lee, S. J.Lin, X. S.Neu, J.Worku, M.Chaaban, M.Ma, B. W.*ACS.Mater.Lett*.2020,**2**,633-638

[21]. Zhang, F.Zhou, Y. C.Chen, Z. P.Wang, M.Ma, Z. Z.Chen, X.Jia, M. C.Wu, D.Xiao, J. W.Li, X. J.Zhang, Y.Shi, Z. F.Shan, C. X.*Advanced Materials*.2022,**34**,12.

[22]. T.T. Xu, Y.Y. Li, M. Nikl, R. Kucerkova, Z.Y. Zhou, J. Chen, Y.Y. Sun, G.D. Niu, J.Tang, Q. Wang, G.H. Ren, Y.T. Wu, *ACS Appl. Mater. Interfaces* 2022, **14**, 14157-14164.

[23]. K. Han, J.C. Jin, B.B. Su, J.W. Qiao, Z.G. Xia, *Advanced Optical Materials*. 2022, **10**, 2200865.

[24]. J.H. Wei, Y.W. Yu, J.B. Luo, Z.Z. Zhang, D.B. Kuang, *Advanced Optical Materials*. 2022, **10**,2200724.

[25]. L.Y. Lian, X. Wang, P. Zhang, J.S. Zhu, X.W. Zhang, J.B. Gao, S. Wang, G.J. Liang,D.L. Zhang, L. Gao, H.S. Song, R. Chen, X.Z. Lan, W.X. Liang, G.D. Niu, J. Tang, J.B.Zhang, *J. Phys. Chem. Lett.* 2021, **12**, 6919-6926.

[26]. B.B.Su,J.C.Jin,K.Han,Z.G.Xia, *Adv.Funct.Mater*.2022,**10**.